Biochimica et Biophysica Acta 1837 (2014) 1801–1809

Contents lists available at ScienceDirect

Biochimica et Biophysica Acta

journal homepage: www.elsevier.com/locate/bbabio

Kinetics of substrate inhibition of periplasmic nitrate reductase

Julien G.J. Jacques [a], Bénédicte Burlat [a], Pascal Arnoux [b], Monique Sabaty [b], Bruno Guigliarelli [a], Christophe Léger [a], David Pignol [b], Vincent Fourmond [a]

[a] Aix-Marseille Université, CNRS, BIP UMR 7281, 31 Chemin J. Aiguier, F-13402 Marseille Cedex 20, France
[b] Aix-Marseille Université, CNRS, CEA, DSV/IBEB/LBC UMR 7265, F-13108 Saint Paul Lez Durance, France

ARTICLE INFO

Article history:
Received 22 January 2014
Received in revised form 14 May 2014
Accepted 22 May 2014
Available online 2 June 2014

Keywords:
Enzyme kinetics
Nitrate reductase
Electrochemistry
EPR spectroscopy

ABSTRACT

Periplasmic nitrate reductase catalyzes the reduction of nitrate into nitrite using a mononuclear molybdenum cofactor that has nearly the same structure in all enzymes of the DMSO reductase family. In previous electrochemical investigations, we found that the enzyme exists in several inactive states, some of which may have been previously isolated and mistaken for catalytic intermediates. In particular, the enzyme slowly and reversibly inactivates when exposed to high concentrations of nitrate. Here, we study the kinetics of substrate inhibition and its dependence on electrode potential and substrate concentration to learn about the properties of the active and inactive forms of the enzyme. We conclude that the substrate-inhibited enzyme never significantly accumulates in the EPR-active Mo(+V) state. This conclusion is relevant to spectroscopic investigations where attempts are made to trap a Mo(+V) catalytic intermediate using high concentrations of nitrate.

1. Introduction

Enzymes of the DMSO reductase family use a mononuclear Mo-bis(pyranopterin guanine dinucleotide) cofactor (MoCo) to catalyze a variety of reactions, mostly transfers of oxo groups [1]. The dissimilatory nitrate reductase (NapAB) from *Rhodobacter sphaeroides* (*Rs*) belongs to the DMSO reductase family and catalyzes the reduction of nitrate into nitrite. It is a 108 kDa, periplasmic, heterodimer which houses a [4Fe-4S] cluster in close proximity to the MoCo, and two surface-exposed, *c*-type hemes [2]. The coordination sphere of the Mo ion consists of the four thiolate ligands of two pyranopterins, a sulfur atom from a cysteine that attaches the MoCo to the protein backbone, and a sixth inorganic ligand, proposed to be oxygen or more recently sulfur [3,2,4,5]. Functional information on nitrate reductase has been obtained mostly from EPR spectroscopy, but this technique is not always conclusive because the EPR signature of the MoCo is heterogeneous, and which signals correspond to species that are actually involved in the catalytic cycle is not entirely clear yet [1].

The heterogeneity of the MoCo is also revealed in direct electrochemistry (or "protein film voltammetry", PFV) experiments [6]. In this technique, *Rs* NapAB is adsorbed onto a rotating pyrolitic graphite edge electrode and the enzyme molecules receive electrons directly from the electrode. When substrate is present in solution, the measured current is proportional to turnover rate. The electrode is spun at a high rate to ensure that there the current is not limited by the diffusion of substrate towards the electrode. The changes in turnover rate in response to changes in experimental conditions (electrode potential, substrate concentration) are instantly detected as changes in current, which makes it very easy to monitor changes in activity resulting from activation or inactivation.

Previously, we used site-directed mutagenesis, EPR and PFV to demonstrate that the MoCo in *Rs* periplasmic nitrate reductase (NapAB) is subject to a slow, *irreversible* reductive activation [7]. The amount of initially inactive form quantitatively correlates with the amount of the so-called "Mo(V) high-*g* resting" EPR signal. More recently, we have proposed that the inactive form features an open, oxidized pyranopterin, which is closed upon reduction [8].

The subject of this paper is a slow, *reversible* inactivation/reactivation process that occurs at high nitrate concentration [9] and is distinct from that reported in ref [8]. Indeed, one is reversible and nitrate concentration-dependent, while the other process is irreversible and independent of nitrate concentration. This inactivation/reactivation is most easily detected in cyclic voltammetry experiments [9], where the electrode potential is repeatedly swept upward and downward to monitor the current/potential response. Fig. 1 shows cyclic voltammograms of *Rs* NapAB recorded at pH 6 and two concentrations of nitrate. According to the conventions we use, a reductive current is negative; therefore, the more negative the current, the higher the turnover rate.

At low nitrate concentration (red trace in Fig. 1), the forward and backward current traces are merely offset by the electrode charging current (dotted black trace). This indicates that catalysis is in a steady-state at each value of the electrode potential. The peculiar wave shape, with a maximum of activity under moderately reducing conditions and a decrease at lower potential, has already been observed with NapAB (from *Rs* [10,11] and *Paracoccus pantotrophus* [12]), and other members

E-mail address: vincent.fourmond@imm.cnrs.fr (V. Fourmond).

http://dx.doi.org/10.1016/j.bbabio.2014.05.357
0005-2728/

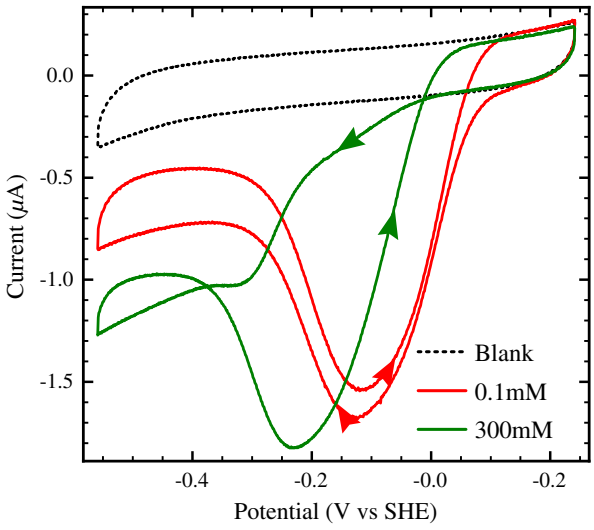

Fig. 1. Cyclic voltammograms of *Rs* NapAB adsorbed onto a rotating PGE electrode. Conditions: pH 6, T = 25 °C, electrode rotation rate $\omega = 5$ krpm, nitrate concentration as indicated. The dotted black line is a blank voltammogram recorded in the absence of enzyme.

of the DMSO reductase family (such as membrane-bound DMSO reductase [13], and respiratory nitrate reductase Nar [14]). Regarding NapAB, a comparison between PFV and solution assays demonstrated that the greater activity in the intermediate range of potential is not an artifact from the electrochemical experiments [15]. The decrease in activity at higher driving force has been attributed to a change in the reaction pathway under more reducing conditions [10,11,13].

At higher nitrate concentrations (green trace in Fig. 1), the voltammogram shows a clear hysteresis: at a given potential, the absolute value of the current, and therefore the activity, is much lower on the sweep towards low potential than on the sweep towards high potential (the arrows in Fig. 1 indicate the direction of the sweeps). This hysteresis reveals a potential-dependent process that is slow on the voltammetric time scale (recording the complete voltammogram takes 80 s).

In a previous work, we showed that this hysteresis stems from a slow potential-dependent inhibition by substrate [9]. In this paper, we characterize in detail the kinetics of inhibition. The information we obtain allows us to compute the proportion of substrate-inhibited species as a function of substrate concentration and potential, and the subfraction of inactive species that are paramagnetic. This analysis will prove crucial to determine if a given spectroscopic signature obtained in turnover conditions is likely to be that of an active species.

2. Results

2.1. Thermodynamics of substrate inhibition: the potential dependence of the inhibition constant

Regarding NapAB, we have shown before [9] that the turnover rate tends to zero at high nitrate concentration, as predicted by the following rate law [16,9]:

$$i = \frac{i_{max}}{1 + K_m/s + s/K_i} \quad (1)$$

where s is the substrate concentration, i_{max} is the maximum current that would be obtained at infinite substrate concentration if there were no inhibition, K_m is the Michaelis constant and K_i the inhibition constant.

The mechanism that gives substrate inhibition in Nap will be discussed below.

It is possible to determine both K_m and the inhibition constant K_i using protein film voltammetry, in an experiment where the electrode potential is held constant and the substrate concentration is increased in a stepwise fashion by repeatedly adding aliquots of a concentrated solution of nitrate. Fig. 2 shows the result of such an experiment, with in panel A the concentration of nitrate as a function of time, and panel B the resulting current. When we carried out this experiment, we waited long enough between each injection for the current to reach its asymptotic value. This steady-state current is plotted against substrate concentration in Fig. 3.

The result in Fig. 3 is consistent with a steady-state current that asymptotically decreases to zero at infinite nitrate concentration, which demonstrates that the nitrate-inhibited form has no residual activity; Eq. (1) is therefore appropriate to fit the data (dotted line).

We repeated the experiment shown in Fig. 2 for different values of the electrode potential (and at two pH values), analyzed the results with Eq. (1), and plotted the values of K_i against potential in Fig. 4. Consistent with our earlier findings that inactivation occurs at high potentials [9], Fig. 4 shows that K_i decreases as the potential increases. In fact, K_i depends on potential in a way consistent with a reaction involving one electron and two nitrate molecules (that is, one decade of K_i per 120 mV). K_i increases only weakly with pH (less than expected for a reaction that would involve 1 proton and two nitrate molecules), which suggests that inhibition is not coupled to a protonation.

Fig. 2 shows that at high substrate concentration (*i.e.* when substrate inhibition occurs) the current relaxes slowly to its steady state value after each addition of nitrate; in contrast, at low substrate concentration, a steady-state is obtained within the mixing time (<1 s). The slow relaxation at high substrate concentration is consistent with the presence of hysteresis in cyclic voltammograms (Fig. 1), and it reveals a transformation that occurs on the voltammetric time scale ($\approx$100 s). This inactivation process is sufficiently slow that it is possible to measure the rate constants of the interconversion between the active (A) and inactive (I) species:

$$A \underset{k_a(E)}{\overset{k_i(E)}{\rightleftharpoons}} I. \quad (2)$$

The knowledge of the apparent inactivation ($k_i(E)$) and reactivation ($k_a(E)$) rate constants is valuable to understand the chemistry of the process. Indeed, the dependence of the rate constants on potential and substrate concentration can reveal the properties of the active and inactive forms as well as the involvement of substrate molecules in the

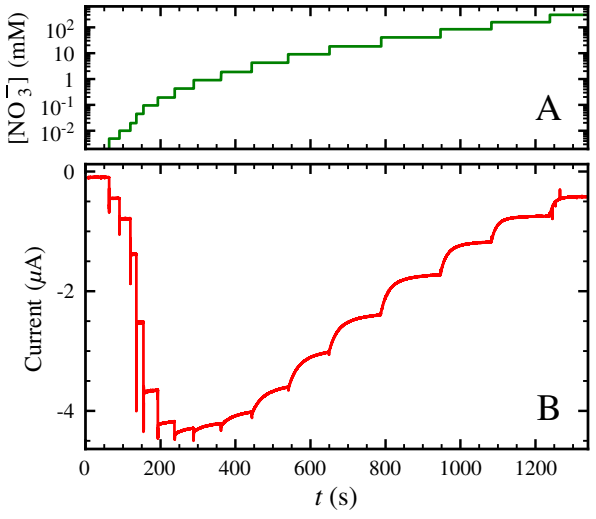

Fig. 2. Chronoamperometric experiment in which an electrode with a film of adsorbed *Rs* NapAB is poised at a constant potential (here −50 mV vs SHE), and various volumes of stock solutions of nitrate are stepwise added into the buffer. Panel A shows the nitrate concentration and panel B the resulting catalytic current.

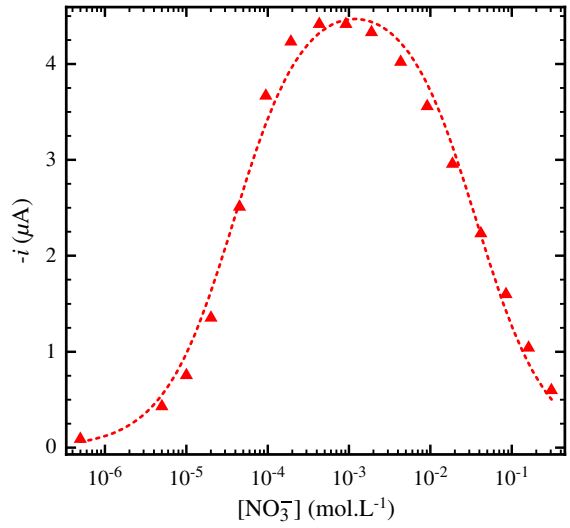

Fig. 3. Steady-state currents of Fig. 2 as a function of nitrate concentration. Film loss was corrected using the method we described earlier [17]. The dotted line shows a fit of Eq. (1) to the data, with parameters $i_{lim} = -4.7$ μA, $K_m = 38$ μM and $K_i = 36$ mM. Note the log scale for abscissa. Conditions: pH 6, 25 °C, potential: −50 mV *vs* SHE.

transformation between active and inactive forms [18,19], as illustrated below.

2.2. Study of transients: a strategy based on potential steps, rather than concentration steps

Two approaches can be used to measure the (in)activation rate constants and their dependence on potential and nitrate concentration.

(i) At a given potential, add substrate in a stepwise fashion (as in Fig. 2), fit an exponential decay to the transients, combine the values of the time constant and the magnitude of the exponential variation (using Eqs. (3)–(6) below) to obtain the rate constants as a function of nitrate for a given potential; repeat for different values of the electrode potential.

(ii) At a fixed concentration, change the potential in a stepwise fashion to monitor the ensuing inactivation or reactivation and deduce the rate constants by fitting an exponential decay to the transients; repeat for several values of the potential to obtain the potential dependence of the rate constants; repeat for different values of the concentration.

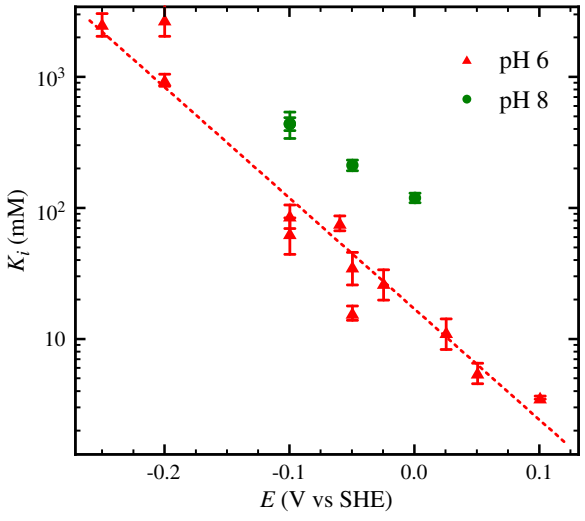

Fig. 4. K_i as a function of potential for two pH values (as indicated). The dashed lines correspond to a slope of 2 nitrate molecules per electron. Temperature 25 °C.

We found that the latter approach (potential steps at a fixed concentration) is the more reliable for several reasons: (i) it is experimentally difficult to repeat the same concentration steps, due to the intrinsic experimental errors in the concentrations (whereas the electrode potential can be set accurately); (ii) the injection of substrate and homogenization of the buffer is not an instantaneous process, even with an electrode spinning at a high rate, and uncontrolled variations in the rates of injection and mixing may affect the transients; and (iii) one can only add substrate, not remove it, which means that one can only obtain transients in the direction of inactivation whereas repeatedly going forward and back between experimental conditions improves the precision with which the rate constants are determined. We therefore chose to perform potential steps at fixed concentration of nitrate to determine the (in)activation rate constants.

2.3. Determination of the inactivation/reactivation rate constants from chronoamperometric experiments

We used a five-step procedure, as illustrated in Fig. 5A. We start with a step at low potential, E_0, long enough to ensure that the enzyme is fully

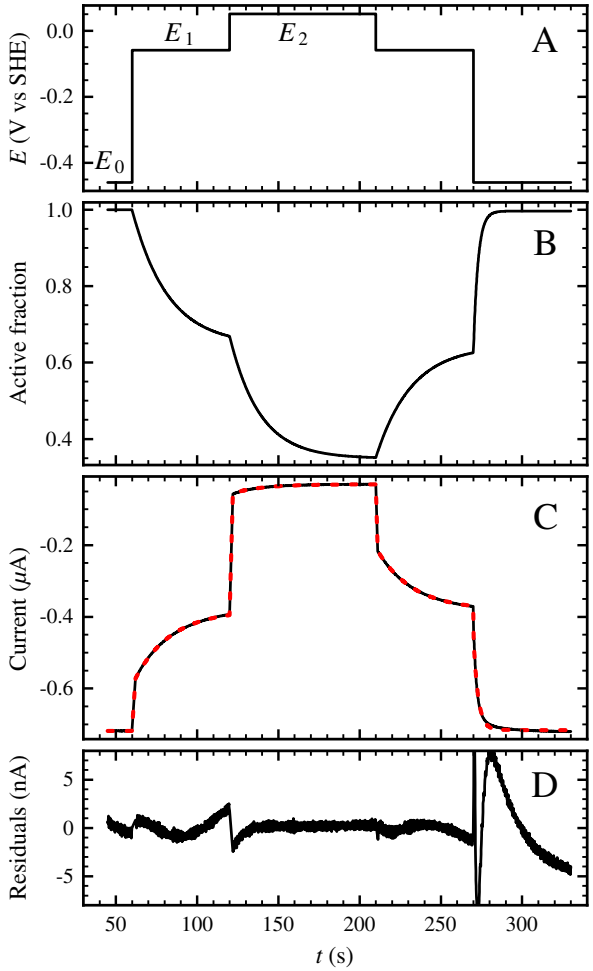

Fig. 5. Chronoamperometric experiments in which an electrode coated with a film of *Rs* NapAB is poised at different potentials in stepwise fashion (panel A). The resulting (blank-subtracted) current is plotted in panel C as a black line, along with a fit using the kinetic model (dashed red line, see text). Panel D shows the residuals of the fit, while panel B shows the evolution of the fraction of active form during the course of the experiment. Conditions: 25 °C, pH 6, 10 mM NO_3^-.

active; we step to an intermediate potential E_1 and then to a higher potential E_2, back to E_1 and E_0. The values of E_1 and E_2 are chosen to ensure that the magnitudes of the inactivation at E_1 and the ensuing reactivation at E_0 are significant.[1] We could fit the current traces using equations derived from the above model (Eq. (2)). The fraction of active form on a step starting at t_0 is given by:

$$A(t) = (A_0 - A_\infty) \times exp(-k_{tot}(t - t_0)) + A_\infty \quad (3)$$

where A_0 is the initial active fraction at $t = t_0$,

$$k_{tot} = k_i(E) + k_a(E) \quad (4)$$

and

$$A_\infty = \frac{k_a(E)}{k_i(E) + k_a(E)}. \quad (5)$$

The current is given by:

$$i(t) = i(E) \times A(t) \times exp[-k_{loss}(E) \times (t - t_0)]. \quad (6)$$

The rightmost term in Eq. (6) accounts for the irreversible desorption of enzymes from the electrode, assuming that it proceeds with a potential-dependent first order rate constant $k_{loss}(E)$. As in our previous works [19,18], we assume that the fractions of active and inactive forms do not instantly change after a potential step: the instantaneous change in current is due to the change in $i(E)$ alone, and the fraction of active enzyme is a continuous function of time (*i.e.* there is no instantaneous inactivation or reactivation). This condition makes it possible to compute the parameter A_0 in Eq. (3) at the beginning of each step, which is necessary for the unambiguous determination of k_i and k_a. With this assumption, we are therefore able to follow the evolution of the fraction of active enzyme as the enzyme (in)activates in response to potential steps (Fig. 5B).

We analyzed a number of chronoamperometric traces such as those in Fig. 5 by adjusting in each case the values of 4 parameters at each potential: $k_i(E)$, $k_a(E)$, $i(E)$ and $k_{loss}(E)$. This model nicely reproduces the data, as attested by the quality of the fit in Fig. 5C and D. We checked by running several fits with different initial conditions that the fits solutions were unique.

A single potential step experiment can be interpreted to obtain the values of k_i and k_a for two potentials (E_1 and E_2) and one concentration of nitrate. Repeating these experiments for different values of the potentials and nitrate concentration (1–100 mM) gave the data points shown in Fig. 6 (at 10 and 50 mM nitrate) and supplementary Fig. S3 (all nitrate concentrations).

The rather large errors on the values of the (in)activation rate constants come from two different experimental limitations. First, at high potential, the current is small, making it difficult to monitor the (in)activation. Second, when either k_i or k_a is more than two orders of magnitude smaller than the other, determining its value requires the reliable detection of changes in activity of less than 1%. The value of k_i is often less accurate than k_a, since the former is always the smaller, except at high potential where the small current impairs the reliable determination of both k_i and k_a.

2.4. The inactive species exists under three redox states

We first focus on the activation rate constants (green markers in Fig. 6). It is important to understand that they report on the *inactive* forms of the enzyme. It is indeed easy to realize that if, for example, we were to observe that the rate of *inactivation* at very low potential is zero, this would imply that the reduced *active* enzyme does not inactivate. In general, studying the dependence of the rate constant of a reaction on experimental conditions informs on the properties of the reactants of the reaction, not on the products.

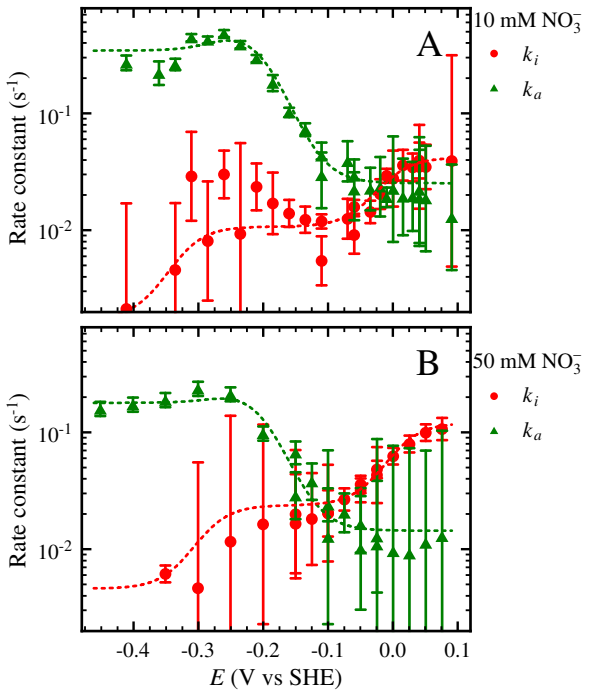

Fig. 6. Rate constants of activation (green) and inactivation (red) as a function of potential for two different nitrate concentrations: 10 mM (panel A) and 50 mM (panel B). Dashed lines are the global fits described later in text, whose parameters are plotted in Fig. 8. Conditions: 25 °C, pH 6.

Fig. 6 shows that the activation rate constant depends on potential; this indicates that the *inactive* species exists under distinct redox states. The bell-shaped dependence on potential further suggests that the inactive species exists in three redox states: an oxidized form that reactivates slowly (*cf* the plateau at high potential), an intermediate form that reactivates quickly (peak at intermediate potential) and a fully reduced form that reactivates a bit more slowly than the intermediate form (low potential plateau). We shall assume that these three forms correspond to the three redox states of the Mo ion (VI, V and IV).

The dependence of k_a on potential can be well described by Eq. (7), which is derived under the assumption that all three redox states are in equilibrium with the electrode, so that the apparent reactivation rate

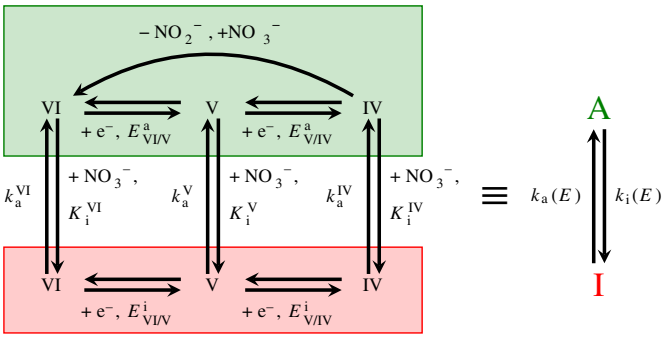

Fig. 7. Kinetic scheme for the inactivation/reactivation process. With the assumption that the different redox states are in equilibrium, the system is equivalent to just two forms that interconvert with apparent rate constants k_a and k_i (rightmost scheme).

[1] While the first step at E_1 is not essential for the determination of the rate constants, it reduces the charging current on the step at E_2 and therefore improves the reliability of the data.

constant is the average of the rate constants of reactivation for each redox state of the inactive species weighted by their respective equilibrium fraction (Fig. 7):

$$k_a(E) = \frac{k_a^{IV} + e_2^i k_a^V + e_1^i e_2^i k_a^{VI}}{1 + e_2^i + e_1^i e_2^i} \quad (7)$$

In this equation k_a^{VI} (resp. k_a^V and k_a^{IV}) are the reactivation rate constants of the most oxidized inactive state (resp intermediate, most reduced), and e_1^i and e_2^i are given by:

$$e_1^i = \exp\left[F\left(E - E_{VI/V}^i\right)/RT\right] \quad (8)$$

$$e_2^i = exp\left[F\left(E - E_{V/IV}^i\right)/RT\right] \quad (9)$$

where we introduced $E_{VI/V}^i$ (resp. $E_{V/IV}^i$), the reduction potential of the VI/V (resp. V/IV) couple of the inactive form (hence the "i" superscript).

2.5. The two redox transitions of the active form can be detected from the dependence on E of the inactivation rate constants

Fig. 6 shows that the inactivation rate constant also depends on potential, which is consistent with the fact that the active form must exist in different redox states within the catalytic cycle. The inactivation rate constant changes in a sigmoidal manner as a function of potential in the high potential region, indicative of a redox transition. The low-potential data points are harder to interpret due to the greater errors on the inactivation rate constants in this region. However, the inactivation rate constants tend to decrease at low potentials for all nitrate concentrations (Figs. 6 and S3): this can be interpreted as the beginnings of a sigmoidal decrease at the potential of the second reduction of the two-electron active site. The potential dependence of the inactivation rate constant can therefore be modeled using the following equation (see Fig. 7 above):

$$k_i(E) = \frac{k_i^{IV} + e_2^a k_i^V + e_1^a e_2^a k_i^{VI}}{1 + e_2^a + e_1^a e_2^a} \quad (10)$$

where k_i^{VI} (resp. k_i^V and k_i^{IV}) are the inactivation rate constants of the most oxidized active state (resp intermediate, most reduced), and e_1^a and e_2^a are given by:

$$e_1^a = \exp\left[F\left(E - E_{VI/V}^a\right)/RT\right] \quad (11)$$

$$e_2^a = \exp\left[F\left(E - E_{V/IV}^a\right)/RT\right] \quad (12)$$

where we introduced $E_{VI/V}^a$ (resp. $E_{V/IV}^a$), the apparent reduction potential of the VI/V (resp. V/IV) couple of the active form (hence the "a" superscript).

2.6. The effect of nitrate

We analyzed the dependence on electrode potential and nitrate concentration of the data in Figs. 6 and S3 using Eqs. (7) and (10). However, instead of adjusting ten parameters at each concentration of nitrate (three activation rate constants, three inactivation rate constants and four redox potentials), we constrained the model as follows.

(i) Regarding the kinetics of the interconversion between the various inhibited species, we chose to adjust the three rate constants of activation and three inhibition constants K_i^{IV}, K_i^V and K_i^{VI} defined by the relation:

$$k_i^{VI} = \frac{[NO_3^-]}{K_i^{VI}} \times k_a^{VI} \quad (13)$$

(and similar equations for the V and IV redox states). The important difference between these two sets of parameters (six rate constants *versus* three rate constants plus three inhibition constants) is that the inhibition constants are independent of the concentration of substrate. Therefore, instead of having to adjust six independent parameters for each substrate concentration, we now have three kinetic parameters for each concentration and a single set of three thermodynamic constants that should take the same values for all concentrations.

(ii) The number of parameters can be further reduced by assuming that the potentials of the redox couples of the inactive form are independent of nitrate concentration, as expected if all redox states of the inactive form have the same number of nitrate molecules bound.

Using these constraints, we fitted the model to the 380 data points (eight distinct concentrations of nitrate spanning two orders of magnitude) adjusting 45 parameters: 5 parameters for each concentration (3 activation rate constants, k_a^{IV}, k_a^V, k_a^{VI} and 2 reduction potentials of the active form) and 5 parameters that are independent of concentration, and whose values are therefore identical for all data sets (the 3 equilibrium constants K_i^{VI}, K_i^V and K_i^{IV}, and the two reduction potentials of the inactive form). While this corresponds to almost half as many parameters as for an unconstrained fit (10 parameters for each of the 8 concentrations), the fits were nearly as good, with the residuals increasing by only 15%. The dashed lines in Figs. 6 and S3 are the results of such constrained fits. The resulting parameters are shown in Fig. 8 and in Table 1. Rate constants as a function of potential for all concentrations along with the global fit are shown in supplementary Fig. S3.

The values in Table 1 show that the affinity for the inhibiting nitrate is two orders of magnitude greater for the VI state than for the V and IV

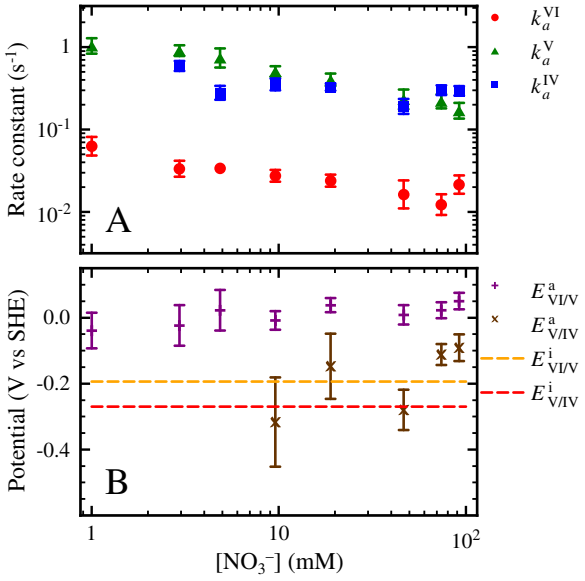

Fig. 8. Results of the global fit of (in)activation rate constants described in the text. Panel A shows the dependence on nitrate concentration of the activation rate constants, while Panel B shows the dependence on nitrate concentration of the reduction potentials of the redox transitions of the active and inactive forms. Equilibrium constants are given in Table 1. The error bars represent the 5% linearized confidence interval of the fit.

Table 1
Values of the nitrate-concentration-independent parameters of the global fit (see text).

Parameter	Value	Error
$E^{i}_{VI/V}$ (V vs SHE)	−0.19	±0.01
$E^{i}_{V/IV}$ (V vs SHE)	−0.27	±0.01
K_i^{IV} (mM)	2000	±400
K_i^{V} (mM)	500	±100
K_i^{VI} (mM)	6	±1

states, the latter having comparable affinities. In other words, the inhibition is more pronounced when the inactive form is in the VI state. The two reduction potentials of the inactive form are close to one another and much lower than the reduction potential of the VI/V couple of the active form (and possibly the V/IV too).

The potential of the VI/V redox transition of the active form could be determined with satisfactory accuracy for most substrate concentrations; it increases slightly as nitrate concentration increases. The potential of the V/IV redox transition of the active form could only be determined for a small number of concentrations.

The activation rate constants could be accurately determined at almost all nitrate concentrations. They would be independent on nitrate concentration *if nitrate binding and release were elementary reactions*. That their values decrease slightly as nitrate concentration increases indicates otherwise. In supplementary section S2, we demonstrate that, under the assumption that intramolecular transport of nitrate is much faster than the inactivation itself, the reactivation rate constant is expected to decrease as nitrate concentration increases. This assumption is reasonable as intramolecular transport of nitrate has to be at least as fast as turnover rates (of the order of 100 s^{-1}), while the rates of inactivation/reactivation never exceed 1 s^{-1}.

Release of nitrate from the VI state is significantly slower than from the V and IV states. Together with the higher affinity of nitrate for the VI state, this indicates that electrostatics probably governs the energetics and kinetics of nitrate binding/release.

2.7. Simulation of experimental voltammograms

With a full kinetic description of the system, we could simulate cyclic voltammograms showing a strong hysteresis, such as the green trace of Fig. 1. We used the same strategy as that described in ref. [19], in which one expresses the current thus:

$$i(E,t) = i(E) \times A(t) \tag{14}$$

where $i(E)$ is the current of the active form as a function of potential and $A(t)$ the fraction of active enzyme as a function of time. Eq. (2) gives the variation in time of the active species:

$$\frac{dA}{dt} = -k_i(E(t)) \times A + k_a(E(t)) \times (1 - A) \tag{15}$$

where $k_i(E)$ and $k_a(E)$ are given by Eqs. (7) and (10). It is not possible to obtain a closed form for $A(t)$, but Eq. (15) is readily integrated by standard numerical techniques.

Having an equation for the current response of the active form, $i(E)$, is another matter altogether. We described previously [10] a model that reproduces faithfully the dependence on potential of the current at low nitrate concentration, but it does not account for the broadening of the catalytic wave observed at higher nitrate concentration [11]. We therefore chose another, self-consistent approach: rather than deriving $i(E)$ from a model, we compute it from the scan towards high potential using Eq. (14) and $A(t)$. The latter is calculated using Eq. (15), with

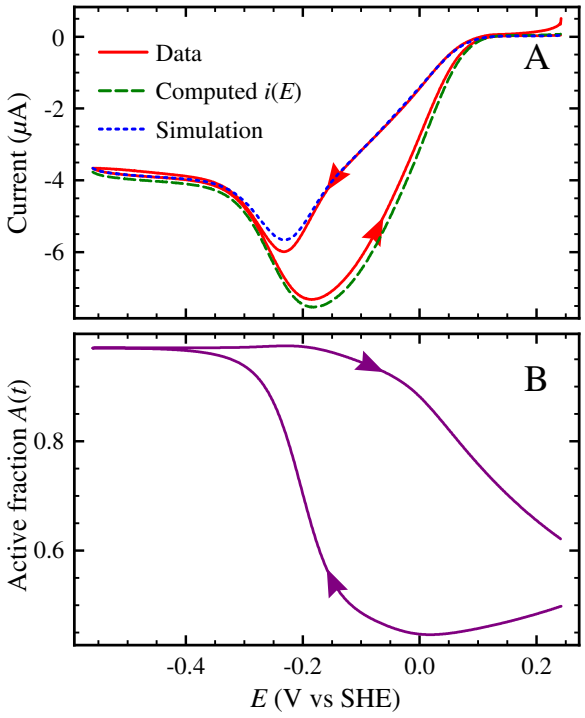

Fig. 9. Simulation of cyclic voltammograms with hysteresis. Conditions: pH 6, T = 25 °C, electrode rotation rate omega = 5 krpm, 10 mM NO_3^-. Panel A: experimental cyclic voltammogram (red trace), $i(E)$ deduced from the scan towards high potentials and calculated $A(t)$ (green dashed trace), simulated scan towards low potentials (blue dotted trace). Panel B: $A(t)$ during the course of the voltammogram, computed by integrating Eq. (15) (purple trace).

the initial condition $A = 1$ (the enzyme is fully active before the electrode potential is swept upward). Knowing $i(E)$ (shown as a green dashed line in Fig. 9B), it is possible to compute the backward scan (dotted blue trace in Fig. 9A). The agreement between the simulated scan and the actual scan is excellent, thereby validating the kinetic model used and the kinetic data obtained by our approach.

2.8. Domain of existence of the paramagnetic inactive species

From the data in Fig. 8 and Table 1, it is possible to compute the fraction of inactive species at pH 6 for a given electrode potential and nitrate concentration:

$$I(E,[NO_3^-]) = \frac{1}{1 + k_a/k_i} = \frac{1}{1 + \frac{k_a^{IV} + e_2^i k_a^V + e_1^i e_2^i k_a^{VI}}{1 + e_2^i + e_1^i e_2^i} \times \frac{1 + e_2^a + e_1^a e_2^a}{k_i^{IV} + e_2^a k_i^V + e_1^a e_2^a k_i^{VI}}} \tag{16}$$

where the values of k_i^{IV}, k_i^V and k_i^{VI} are determined for each concentration of nitrate by using Eq. (13). The steady-state fraction of inactive enzyme is plotted as contour lines in Fig. 10A. The values of K_i obtained earlier (Fig. 4) are shown as triangles in the same figure. They overlay well the 50% contour (purple line), showing that the results of the potential steps approach are consistent with the inhibition constants determined using "concentration steps" (Figs. 2 and 3).

Furthermore, it is possible to compute the steady-state fraction of inactive species that is in the Mo(V) state from the values of the redox potentials of the inactive form (Table 1) combined with Eq. (16). This gives the overall concentration of inactive Mo(V) species:

$$I_V(E,[NO_3^-]) = \frac{e_2^i}{1 + e_2^i + e_1^i e_2^i} \times I(E,[NO_3^-]). \tag{17}$$

This is shown as contour lines in Fig. 10B.

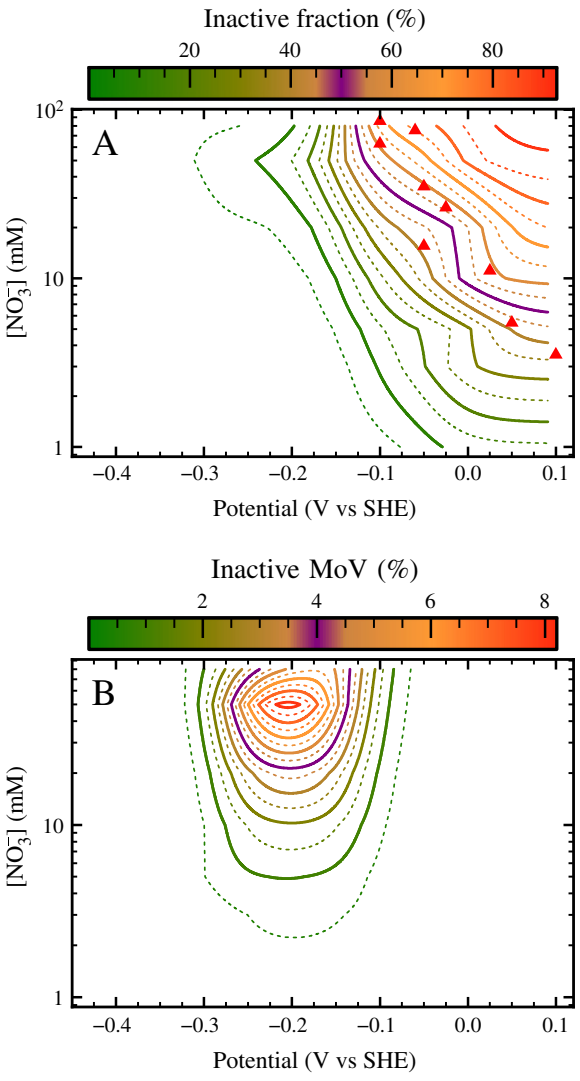

Fig. 10. Panel A: steady-state fraction of the enzyme that is in the inactive form as a function of nitrate concentration and potential, pictured as contour lines; solid lines correspond to multiples of 10%. The purple level lines correspond to 50% inactive form. The red triangles are the values of K_i at pH 6 (replotted from Fig. 4). Panel B: steady-state fraction of the enzyme that is in the paramagnetic state of the inactive form as a function of potential and substrate concentration, pictured as contour lines; solid lines correspond to multiples of 1%. The purple level line corresponds to 4% MoV. Conditions: pH 6, 25 °C.

The maximum of fraction of inactive MoV is about 8% for a very narrow region around −200 mV and 50 mM nitrate but its concentration rapidly decreases outside of that region, to amount to less than 4% at 20 mM nitrate whatever the value of E (the 4% level line is drawn in purple in Fig. 10B). On the other hand, the fraction of enzyme in the inactive form increases steadily with increasing potential and/or nitrate, to exceed 80% at potentials above 0 V and nitrate concentration above 20 mM.

Given the high experimental uncertainty in the value of $E^a_{V/IV}$ and its presence in the expression of $I(E,[NO_3^-])$ (and, hence $I_V(E,[NO_3^-])$) *via* the e_2^a term in Eq. (16), we sought to assess the impact of this uncertainty on the maps of Fig. 10. We have therefore studied the influence of its variation on the calculated fraction of inactive Mo(V) species (supplementary Fig. S4). We show that, even if $E^a_{V/IV}$ were as low as -400 mV for all nitrate concentrations, the total amount of inactive Mo(V) would only increase to 12%, but at higher nitrate concentrations (at the same potential). Changing the reduction potential does not significantly extend of the region in which the concentration of inactive Mo(V) is greater than 4%. It is important to emphasize that the value of $E^a_{V/IV}$ is unlikely to be that low, as all reduction potentials values determined with reasonable accuracy from Fig. 8 are much higher than that (about −200 mV).

Using the same approach, we wanted to determine the fraction of active species in the Mo(V) state as a function of potential and nitrate concentration. While this would be desirable in order to design experiments that maximize the chances to trap active paramagnetic species, this was unfortunately not feasible from our data. Indeed, if the value of the $E^a_{V/IV}$ potential does not affect the concentration of *inactive* Mo(V) as demonstrated above, it directly affects the stability range of the *active* Mo(V). With the experimental uncertainty on $E^a_{V/IV}$, the fraction of active Mo(V) cannot be accurately determined.

3. Discussion

Periplasmic nitrate reductase adsorbed at a graphite electrode gives a voltammetric signal (Fig. 1) where the already complex steady-state catalytic response is distorted by a reversible, slow, redox- and substrate concentration-dependent (in)activation process [9]. Cyclic voltammograms showing a hysteresis that results from a reversible inactivation process have been recorded before by PFV for several enzymes: NiFe [20,19] and FeFe hydrogenases [21,18]. This was also observed with horseradish peroxydase using mediated electrochemistry [22]. The case of nitrate reductase is particularly intriguing since neither the structure of the inactive state nor the mechanism of inhibition are known. The observation that the enzyme is inhibited by its substrate has consequences on the design of experiments where one tries to trap and characterize catalytic intermediates. It is essential to find out whether or not the substrate-inhibited form of the enzyme is one of the species that has been isolated and characterized using EPR. Our goal was therefore two-fold. We aimed at quantitatively analyzing the electrochemical data to learn about the (in)activation process and obtain molecular information about the inactive state(s). We also wanted to better define which experimental conditions are best suited to accumulate catalytic intermediates and avoid inactive species.

We used the strategy that we recently developed for studying the reversible redox-driven (in)activation of NiFe and FeFe hydrogenases [19,18]. The activity of the enzyme is monitored as a function of time, in an experiment where the electrode potential is repeatedly stepped up and down to trigger inactivation and reactivation (Fig. 5). The data are fitted using a simple two-state model (Eq. (2)), where the active and inactive forms of the enzyme interconvert with apparent rate constants k_i and k_a. The dependence on potential (Fig. 6) and nitrate concentration (Fig. 8) of these two apparent rate constants is interpreted to learn about the different redox states of the active and inactive states, and how they interconvert (Fig. 7). This analysis shows that the potential dependence of the inactivation stems from the fact that the inhibiting nitrate has a much higher affinity for the VI state of the enzyme rather than the more reduced states V and IV.

The information we gained is summarized in the two contour plots of Fig. 10, where we show the steady-state fraction of the enzyme that is in the inactive form as a function of nitrate concentration and potential (panel A) and the steady-state fraction of the enzyme that is in the paramagnetic state of the inactive form as a function of potential and substrate concentration (panel B).

The map in Fig. 10A shows that, as emphasized in our earlier work [9], inactive forms of the enzyme accumulate at high potentials and high concentrations of nitrate. However, by combining the information in Fig. 10A and B, we conclude that the substrate-inhibited states accumulate mostly in the EPR-silent Mo(VI) state. This is a consequence of the inhibition constant being much lower for the VI state than for the other redox states (Table 1). At pH 6 and nitrate concentrations below 100 mM, the fraction of EPR-active substrate-inhibited enzyme is expected to be lower than 10%, regardless of the potential.

Regarding the experiments aimed at trapping catalytic intermediates in solution, carried out at very high concentration of nitrate, we

conclude that the risk of mistaking an Mo(V) signal of the substrate-inhibited form for a catalytically active species is actually low. However, unless very reducing conditions are employed, the use of a high concentration of nitrate favors the accumulation of the inactive form, which decreases the chances of detecting a catalytically competent EPR-active state. As a consequence, concentrations of nitrate above 10 mM should be avoided.

As explained in *e.g.* section 5.9.1 of ref. [16], substrate inhibition cannot result from the non-productive binding of nitrate in a manner that prevents (or competes with) normal binding. Substrate inhibition is usually rationalized in terms of a second molecule of substrate binding to the enzyme-substrate complex (idem, section 5.9.2). This led us to label the substrate inhibited species as "Mo-S2" (*i.e.* active site bound to two molecules of substrate) in our earlier work [9]. However, we show in SI section S1 that substrate inhibition may also occur if, in the catalytic cycle, a substrate molecule binds the enzyme between the release of the product and the return of the enzyme to its "resting state" (we define the resting state as the form of the enzyme that accumulates in the absence of substrate): two molecules of substrate are needed for substrate inhibition, but they do not necessarily exist at the same time in the active site pocket. This situation has also been described for dimeric glucose oxidase [23].

Several aspects of the catalytic cycle of Nap remain to be elucidated, but it is commonly accepted that nitrate binds to the active site through one of the oxygen atoms, which is retained as an oxo or hydroxo group upon release of nitrite, and must be removed before another nitrate molecule can bind to start the next catalytic cycle [24]. We observed that inhibition by nitrate in Nap is very sensitive to the redox state of the active site (Table 1), which indicates that the inhibiting molecule of nitrate binds either at, or very close to, the active site. Since the active site cavity is too small to simultaneously accommodate two molecules of nitrate, we consider as most likely that inhibition results from a molecule of nitrate entering the cavity after nitrite has been released, but before the remaining oxo group has detached from the active site. According to this hypothesis, the inhibiting nitrate would prevent the release of the oxo group, thus blocking the enzyme in a state that is a dead-end species because it cannot bind nitrate (this state is named E′S in supplementary Fig. S2). This mechanism is likely to be specific of periplasmic Nap; indeed, substrate inhibition has never been reported with the related membrane-bound, respiratory nitrate reductases (NarGHI), and despite an extensive search, we could not evidence nitrate inhibition in the case of *Escherichia coli* NarGHI (unpublished results). The coordination sphere of the Mo in Nap is different from that in Nar (a cystein binds the Mo in NapA, it is an aspartate in NarG), and this may impact both the nature of the catalytic intermediates and the existence of dead-end, substrate-inhibited states.

Many Mo(V) EPR signatures of periplasmic nitrate reductases have been reported [7,3,8]. The most studied are those from the so-called "high-*g*" family ("high-*g* resting", "high-*g* nitrate" and "high-*g* turnover"). According to DFT investigations, their EPR spectra are consistent with a Mo coordinated by 6 sulfur ligands [3]. We recently proposed that the "high-*g* resting" signal arises from an inactive species where one pyranopterin is open and therefore non-functional [8]. The implication in the catalytic cycle of the species that give the "high-*g* nitrate" and "high-*g* turnover" signals has been proposed based on the observation that they are formed during turnover conditions [25,26], but the argument is actually weak, since the present study and earlier works [9] show that, even in turnover conditions, inactive species can accumulate to a significant extent. Clearly, that a species is formed only in turnover conditions does not imply that it is catalytically relevant. However, the detailed analysis herein suggested that the inactive form of Nap that accumulates under very high concentrations of nitrate is not present in the intermediate (Mo(V)) redox state, and therefore does not correspond to a species that has been detected by EPR before.

4. Conclusion

Using electrochemical potential step techniques, we were able to characterize the kinetic and thermodynamic aspects of the potential-dependent substrate inhibition of periplasmic nitrate reductase. We have shown that in the inhibited form, the affinity for nitrate is much greater for the Mo VI state than for the V and IV states. We could precisely define the experimental conditions (in terms of potential and nitrate concentration) where the inactive forms accumulate, and which portion of it is in a paramagnetic state. We found that inactive species do accumulate at high nitrate concentration, but not in a paramagnetic form. This will be useful for designing experiments aimed at trapping and characterizing catalytic intermediates.

5. Methods

5.1. Purification of NapAB

Samples of *R. sphaeroides f. sp. denitrificans* IL106 NapAB were purified as previously described [2].

5.2. Protein film voltammetry experiments

The electrochemical setup was the same as that described in refs. [7,9]. It consisted of a pyrolytic graphite edge (PGE) rotating electrode, a saturated calomel reference electrode and a platinum counter electrode. Before each measurement, the PGE electrode was abraded with α alumina (Buehler), sonicated, rinsed and dried. 0.6 μL of a 0.2 M neomycin sulfate solution was then deposited on the electrode, allowed to dry for 5 min. 0.6 μL of a stock solution of NapAB was deposited and allowed to dry. The electrolytic solution, buffered with (2-(N-morpholino) ethanesulfonic acid) MES, (N-cyclohexyl-2- aminoethanesulfonic acid) CHES, (2-[4-(2-hydroxyethyl)piperazin-1-yl] ethanesulfonic acid) HEPES, (3-[[1,3-dihydroxy-2-(hydroxymethyl)propan-2-yl] amino] propane-1-sulfonic acid) TAPS and sodium acetate (5 mM each), contained 0.1 M sodium chloride.

5.3. Data analysis

We analyzed and fitted the data using in-house programs called SOAS [27] and QSoas. The former is available free of charge on our Web site at `http://bip.cnrs-mrs.fr/bip06/software.html`. It is being replaced by an entirely new, powerful, open-source program called QSoas, which will become available soon. Both programs embed the ODRPACK software for non-linear least squares regressions [28]. For the measurement of K_i, we corrected film loss as illustrated with the experiments aimed at measuring K_m in ref. [17]. The data were plotted using `ctioga2` (`http://ctioga2.sourceforge.net`).

Acknowledgments

The authors wish to thank Pierre Ceccaldi for carrying out the search for inactivation by substrate on the E. coli NarGHI enzyme. This work was funded by the CNRS, CEA, Aix-Marseille Université and the Agence Nationale de la Recherche (ANR MC2 n°11-BSV5-005-01).

Appendix A. Supplementary data

Supplementary data and equations to this article can be found online at http://dx.doi.org/10.1016/j.bbabio.2014.05.357.

References

[1] S. Grimaldi, B. Schoepp-Cothenet, P. Ceccaldi, B. Guigliarelli, A. Magalon, The prokaryotic Mo/W-bisPGD enzymes family: a catalytic workhorse in bioenergetics, Biochim. Biophys. Acta 1827 (8–9) (2013) 1048–1085, http://dx.doi.org/10.1016/j.bbabio.2013.01.011.

[2] P. Arnoux, M. Sabaty, J. Alric, B. Frangioni, B. Guigliarelli, J.-M. Adriano, D. Pignol, Structural and redox plasticity in the heterodimeric periplasmic nitrate reductase, Nat. Struct. Mol. Biol. 10 (11) (2003) 928–934, http://dx.doi.org/10.1038/nsb994.
[3] F. Biaso, B. Burlat, B. Guigliarelli, DFT investigation of the molybdenum cofactor in periplasmic nitrate reductases: structure of the Mo(V) EPR-active species, Inorg. Chem. 51 (2012) 3409–3419, http://dx.doi.org/10.1021/ic201533p.
[4] S. Najmudin, P. González, J. Trincão, C. Coelho, A. Mukhopadhyay, N. Cerqueira, C. Romão, I. Moura, J. Moura, C. Brondino, M. Romão, Periplasmic nitrate reductase revisited: a sulfur atom completes the sixth coordination of the catalytic molybdenum, J. Biol. Inorg. Chem. 13 (5) (2008) 737–753, http://dx.doi.org/10.1007/s00775-008-0359-6.
[5] C. Coelho, P.J. González, J.G. Moura, I. Moura, J. Trincão, M. João Romão, The crystal structure of *Cupriavidus necator* nitrate reductase in oxidized and partially reduced states, J. Mol. Biol. 408 (5) (2011) 932–948, http://dx.doi.org/10.1016/j.jmb.2011.03.016.
[6] C. Léger, P. Bertrand, Direct electrochemistry of redox enzymes as a tool for mechanistic studies, Chem. Rev. 108 (7) (2008) 2379–2438, http://dx.doi.org/10.1021/cr0680742.
[7] V. Fourmond, B. Burlat, S. Dementin, P. Arnoux, M. Sabaty, S. Boiry, B. Guigliarelli, P. Bertrand, D. Pignol, C. Léger, Major Mo(V) EPR signature of *Rhodobacter sphaeroides* periplasmic nitrate reductase arising from a dead-end species that activates upon reduction. Relation to other molybdoenzymes from the DMSO reductase family, J. Phys. Chem. B 112 (48) (2008) 15478–15486.
[8] J.G. Jacques, V. Fourmond, P. Arnoux, M. Sabaty, E. Etienne, S. Grosse, F. Biaso, P. Bertrand, D. Pignol, C. Léger, B. Guigliarelli, B. Burlat, Reductive activation in periplasmic nitrate reductase involves chemical modifications of the Mo-cofactor beyond the first coordination sphere of the metal ion, Biochim. Biophys. Acta Bioenerg. 1837 (2) (2014) 277–286, http://dx.doi.org/10.1016/j.bbabio.2013.10.013.
[9] V. Fourmond, M. Sabaty, P. Arnoux, P. Bertrand, D. Pignol, C. Léger, Reassessing the strategies for trapping catalytic intermediates during nitrate reductase turnover, J. Phys. Chem. B 114 (9) (2010) 3341–3347.
[10] B. Frangioni, P. Arnoux, M. Sabaty, D. Pignol, P. Bertrand, B. Guigliarelli, C. Léger, In *Rhodobacter sphaeroides* respiratory nitrate reductase, the kinetics of substrate binding favors intramolecular electron transfer. J. Am. Chem. Soc. 126 (5) (2004) 1328–1329.
[11] P. Bertrand, B. Frangioni, S. Dementin, M. Sabaty, P. Arnoux, B. Guigliarelli, D. Pignol, C. Léger, Effects of slow substrate binding and release in redox enzymes: theory and application to periplasmic nitrate reductase, J. Phys. Chem. B 111 (34) (2007) 10300–10311.
[12] A.J. Gates, D.J. Richardson, J.N. Butt, Voltammetric characterization of the aerobic energy-dissipating nitrate reductase of *Paracoccus pantotrophus*: exploring the activity of a redox-balancing enzyme as a function of electrochemical potential, Biochem. J. 409 (1) (2008) 159–168, http://dx.doi.org/10.1042/BJ20071088.
[13] K. Heffron, C. Léger, R. Rothery, J. Weiner, F. Armstrong, Determination of an optimal potential window for catalysis by *E. coli* dimethyl sulfoxide reductase and hypothesis on the role of Mo(V) in the reaction pathway, Biochemistry 40 (10) (2001) 3117–3126, http://dx.doi.org/10.1021/bi002452u.
[14] L. Anderson, D. Richardson, J. Butt, Catalytic protein film voltammetry from a respiratory nitrate reductase provides evidence for complex electrochemical modulation of enzyme activity, Biochemistry 40 (38) (2001) 11294–11307, http://dx.doi.org/10.1021/bi002706b.
[15] V. Fourmond, B. Burlat, S. Dementin, M. Sabaty, P. Arnoux, E. Étienne, B. Guigliarelli, P. Bertrand, D. Pignol, C. Léger, Dependence of catalytic activity on driving force in solution assays and protein film voltammetry: insights from the comparison of nitrate reductase mutants, Biochemistry 49 (11) (2010) 2424–2432, http://dx.doi.org/10.1021/bi902140e.
[16] A. Cornish-Bowden, Fundamentals of Enzyme Kinetics, 3rd edition Portland Press, 2004, ISBN 1 85578 1581. (URL http://bip.cnrs-mrs.fr/bip10/fek.htm).
[17] V. Fourmond, T. Lautier, C. Baffert, F. Leroux, P.-P. Liebgott, S. Dementin, M. Rousset, P. Arnoux, D. Pignol, I. Meynial-Salles, P. Soucaille, P. Bertrand, C. Léger, Correcting for electrocatalyst desorption or inactivation in chronoamperometry experiments, Anal. Chem. 81 (8) (2009) 2962–2968.
[18] V. Fourmond, C. Greco, K. Sybirna, C. Baffert, P.-H. Wang, P. Ezanno, M. Montefiori, M. Bruschi, I. Meynial-Salles, P. Soucaille, J. Blumberger, H. Bottin, L. De Gioia, C. Léger, The oxidative inactivation of FeFe hydrogenase reveals the flexibility of the H-cluster, Nat. Chem. 6 (4) (2014) 336–342, http://dx.doi.org/10.1038/nchem.1892.
[19] V. Fourmond, P. Infossi, M.-T. Giudici-Orticoni, P. Bertrand, C. Léger, Two-step" chronoamperometric method for studying the anaerobic inactivation of an oxygen tolerant NiFe hydrogenase, J. Am. Chem. Soc. 132 (13) (2010) 4848–4857.
[20] A. Jones, S. Lamle, H. Pershad, K. Vincent, S. Albracht, F. Armstrong, Enzyme electrokinetics: electrochemical studies of the anaerobic interconversions between active and inactive states of *Allochromatium vinosum* [NiFe]-hydrogenase, J. Am. Chem. Soc. 125 (28) (2003) 8505–8514, http://dx.doi.org/10.1021/ja035296y.
[21] A. Parkin, C. Cavazza, J. Fontecilla-Camps, F. Armstrong, Electrochemical investigations of the interconversions between catalytic and inhibited states of the [FeFe]-hydrogenase from *Desulfovibrio desulfuricans*, J. Am. Chem. Soc. 128 (51) (2006) 16808–16815, http://dx.doi.org/10.1021/ja064425i.
[22] M. Dequaire, B. Limoges, J. Moiroux, J.-M. Savéant, Mediated electrochemistry of horseradish peroxidase. Catalysis and inhibition. J. Am. Chem. Soc. 124 (2) (2002) 240–253.
[23] F. Durand, B. Limoges, N. Mano, F. Mavré, R. Miranda-Castro, J.-M. Savéant, Effect of substrate inhibition and cooperativity on the electrochemical responses of glucose dehydrogenase. Kinetic characterization of wild and mutant types, J. Am. Chem. Soc. 133 (2011) 12801–12809, http://dx.doi.org/10.1021/ja204637d.
[24] C. Sparacino-Watkins, J.F. Stolz, P. Basu, Nitrate and periplasmic nitrate reductases, Chem. Soc. Rev. 43 (2014) 676–706, http://dx.doi.org/10.1039/C3CS60249D.
[25] C. Butler, J. Charnock, B. Bennett, H. Sears, A. Reilly, S. Ferguson, C. Garner, D. Lowe, A. Thomson, B. Berks, D. Richardson, Models for molybdenum coordination during the catalytic cycle of periplasmic nitrate reductase from *Paracoccus denitrificans* derived from EPR and EXAFS spectroscopy, Biochemistry 38 (28) (1999) 9000–9012, http://dx.doi.org/10.1021/bi990402n.
[26] P. Gonzàlez, M. Rivas, C. Brondino, S. Bursakov, I. Moura, J. Moura, EPR and redox properties of periplasmic nitrate reductase from *Desulfovibrio desulfuricans* ATCC 27774, J. Biol. Inorg. Chem. 11 (5) (2006) 609–616, http://dx.doi.org/10.1007/s00775-006-0110-0.
[27] V. Fourmond, K. Hoke, H.A. Heering, C. Baffert, F. Leroux, P. Bertrand, C. Léger, Soas: a free program to analyze electrochemical data and other one-dimensional signals, Bioelectrochemistry 76 (1–2) (2009) 141–147.
[28] P.T. Boggs, J.R. Donaldson, R.H. Byrd, R.B. Schnabel, Algorithm 676: Odrpack: software for weighted orthogonal distance regression, ACM Trans. Math. Softw. 15 (4) (1989) 348–364, http://dx.doi.org/10.1145/76909.76913.